

Dissipative Phase Transition in a Parametrically Amplified Quantum Rabi Model with Two-photon decay

Mingjian Zhu* and Han Pu†

Department of Physics and Astronomy, and Smalley-Curl Institute, Rice University, Houston, TX 77005, USA

(Dated: March 20, 2026)

We investigate dissipative phase transitions (DPTs) in a parametrically amplified open quantum Rabi model (QRM) with both single- and two-photon decay. In the classical oscillator limit, four composite phases emerge, arising from the possible normal or superradiant regimes across the upper and lower spin branches. A mean-field analysis reveals an “inverted” regime where superradiance emerges only at sufficiently low spin-boson coupling. This regime features first- and second-order DPTs separated by a tricritical point, while two-photon dissipation preserves the stability of the superradiant phase. Utilizing an adiabatic approach and the semi-classical Langevin formalism, we further study the steady-state structure beyond the mean-field level. We show that the tricriticality stems from the intrinsic nonlinearity of QRM, unveiled by the interplay of coherent and dissipative two-photon processes. The universality classes of the DPTs are identified, with the corresponding critical and finite-size scaling exponents derived and a scaling ansatz proposed to describe the critical behavior.

Introduction – The quantum Rabi model (QRM) represents a fundamental paradigm in quantum optics, as it encodes the light–atom interaction with the minimal set of degrees of freedom [1–3]. The QRM and its multi-atom extension, the quantum Dicke model (QDM), are well-known for exhibiting the second-order superradiant quantum phase transition [4, 5]. Significant attention has also been paid to dissipative phase transitions (DPTs), the non-equilibrium generalization of quantum phase transitions, characterized by non-analytical changes in the steady state [6–11]. In addition to their intrinsic physical importance, DPTs can be utilized as robust quantum resources for metrology and error correction applications [12–15]. Second-order superradiant DPTs have been identified in both open QRM and QDM with single-photon decay [16, 17] and experimentally observed across various quantum simulation platforms [18–23]. Beyond typical models, theoretical studies of generalized QRMs and QDMs—variants incorporating complex interactions or modified level structures—have revealed a richer critical phenomenon, including first-order transitions and tricriticality [24–32].

Although prior research on these generalized models focuses primarily on coherent interactions, the influence of dissipative mechanisms on DPTs has emerged as a subject of growing interest [33–35]. The state-of-the-art quantum simulation techniques have now enabled the precise engineering of dissipation with high complexity, leading to new regimes of non-equilibrium physics [36–42]. In particular, the two-photon decay, the quantum analogy of the nonlinear damping in a classical van der Pol oscillator [43, 44], exhibits distinctive features of interest [45–47]. In photonic systems, it has been shown to stabilize parametric amplified oscillators [48, 49] and induce second-order DPTs in Kerr oscillators [50]. Recent studies reveal that it gives rise to interesting physics in light-atom-interacting systems, ranging from parity-

dependent non-Hermitian dynamics in the QRM [51, 52] to the stabilization of superradiance in the two-photon QDM [53].

In this paper, we present a comprehensive study of the influence of two-photon dissipation on the DPTs exhibited by the open QRM. To incorporate both coherent and dissipative two-photon mechanisms, we add a parametric amplification (PA) to the Rabi Hamiltonian, which is commonly used for creating bosonic squeezing [54, 55] and accelerating quantum gates [56]. Using a mean-field (MF) theory, we show that the PA extends the DPTs to both the upper and lower spin branches, yielding four steady-state phases, in contrast to the standard QMR where the transition is restricted to the lower spin branch [16]. Notably, we identify an “inverted” regime in which superradiance emerges when the spin-boson coupling is tuned below a critical value, in stark contrast to the standard QRM/QDM where the superradiant phase is accessed when the coupling is sufficiently large. In this regime, the lower branch supports both first- and second-order DPTs separated by a tricritical point (TCP). We then step beyond the MF theory and obtain an analytic expression of the steady-state Wigner function. This formalism reveals that the TCP originates from the intrinsic nonlinearity of the QRM, driven by the interplay of PA and two-photon decay. Finally, we confirm the tricritical nature of the system by extracting scaling laws for two distinct universality classes and construct a scaling ansatz to describe the finite-size crossover regime.

The Model – Our Rabi Hamiltonian with PA reads:

$$H = \frac{\Omega}{2}\sigma_z + \omega_0 a^\dagger a + \frac{\mu}{2}\omega_0(a^2 + a^{\dagger 2}) + \lambda\sigma_x(a + a^\dagger), \quad (1)$$

where μ is the strength of the PA. The system is subject to both one- and two-photon Markovian dissipation and its dynamics can be described by a Lindblad master equation [57]:

$$\partial_t \rho = \mathcal{L}\rho = -i[H, \rho] + 2\kappa_1 \mathcal{D}_a[\rho] + 2\kappa_2 \mathcal{D}_{a^2}[\rho], \quad (2)$$

with $\mathcal{D}_c[\rho] = c\rho\dot{c} + \frac{1}{2}\{c^\dagger c, \rho\}$. Following the notation in Ref. [16], we have denoted the rates of one- and two-photon decay as $2\kappa_1, 2\kappa_2$, respectively.

Mean-field Theory – We first solve the steady-state observables using the MF theory, which is precise in the thermodynamic limit (TDL). We renormalize the two-photon decay rate by defining $\kappa_2 \equiv \gamma_2\omega_0/\eta$, where γ_2 is a dimensionless constant and $\eta \equiv \Omega/\omega_0$. Here the TDL is defined by taking the classical oscillator limit $\eta \rightarrow \infty$ while keeping γ_2 finite. The steady state then factorizes into the product of a spin state and a coherent bosonic state, since the spin and bosonic degrees of freedom are effectively decoupled while the photon number $\langle n \rangle$ diverges [14, 16, 50]. With $\bar{\alpha} = \langle a \rangle / \sqrt{\eta} = (\bar{x} + i\bar{p})/\sqrt{2}$, the corresponding steady-state Heisenberg equations can be written as (see Appendix A for details):

$$\begin{aligned} 0 &= (1 - \mu)\bar{p} - \gamma_1\bar{x} - \gamma_2(\bar{x}^2 + \bar{p}^2)\bar{x}, \\ 0 &= -(1 + \mu)\bar{x} \mp f_{\text{nl}}(\bar{x}) - \gamma_1\bar{p} - \gamma_2(\bar{x}^2 + \bar{p}^2)\bar{p}. \end{aligned} \quad (3)$$

where $\gamma_1 \equiv \kappa_1/\omega_0$, $g \equiv 2\lambda/\sqrt{\omega_0\Omega}$, and we have defined $f_{\text{nl}}(x) = g^2x(2g^2x^2 + 1)^{-1/2}$ as an effective nonlinear force that encodes the spin-boson coupling. The corresponding steady-state spin polarization takes two different values $s_z = \langle \sigma_z \rangle = \pm(2g^2\bar{x}^2 + 1)^{-1/2}$, defining two spin branches which we will denote as the upper (+) and the lower (-) branches. The \mp signs in front of f_{nl} are associated with the (+), (-) branches, respectively. The fact that γ_2 is finite, hence $\kappa_2 \propto \eta^{-1}$, ensures that Eq. (3) remains a valid MF equation independent of η [53, 58]. In arriving at Eq. (3), we have mapped our open QRM to a nonlinear dynamical system.

We introduce the normalized steady-state photon number $\bar{n}_{ss} = \langle n \rangle(t \rightarrow \infty)/\eta$ as the order parameter, with its mean-field value $\bar{n}_{\text{mf}} = |\bar{\alpha}|^2$. $\bar{n}_{\text{mf}} = 0$ or > 0 define the normal (NP) and the superradiant phase (SRP), respectively. The SRP parameter space is determined by the existence of stable non-trivial solutions (\bar{x}_s, \bar{p}_s) of Eq. (3). To track their emergence, we expand $f_{\text{nl}}(x)$ to the order of $2N + 1$ in x and construct a function $F_{\pm}(x) = \sum_{n=0}^{2N+3} c_{2n}^{\pm} x^{2n}$ such that $dF_{\pm}(\bar{x})/d\bar{x} = 0$ yields the equivalent MF equation satisfied by \bar{x} (see Appendix A for derivations). We shall show later with the Langevin formalism that $F_{\pm}(x)$ can be mapped to an effective potential. The set of coefficients c_{2n}^{\pm} then allows us to extract critical points of all orders through the Landau theory. The sufficient condition for the SRP is obtained by requiring the trivial solution to be unstable:

$$c_2^{\pm} = (1 - \mu)(1 + \mu \pm g^2) + \gamma_1^2 < 0. \quad (4)$$

For the same set of parameters, the two spin branches may exhibit different phases, resulting in a total of four phases, as shown by the example phase diagram in Fig. 1(a), where the dashed and solid lines correspond to the second- and first-order phase boundaries, respec-

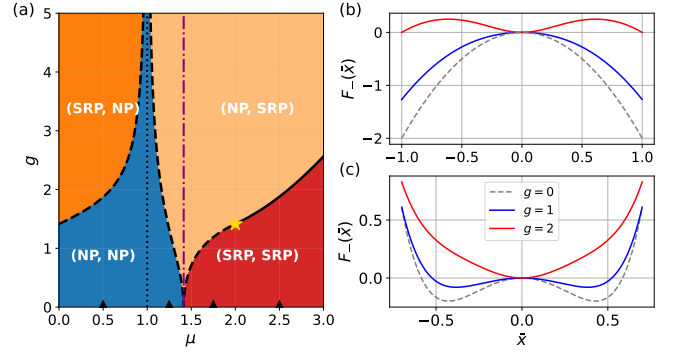


Figure 1: **(a)** Phase diagram in the (μ, g) parameter space with $\gamma_1 = \gamma_2 = 1$. In each regime the phases of the (\pm) spin branches are listed in the order {phase (-), phase (+)}. The dashed (solid) black curves marks the critical condition for DPTs of second- (first-)order. The TCP at $(\mu = 2, g = \sqrt{2})$ is highlighted by a yellow star. The purple dot-dashed line at μ_c marks the boundary of the inverted regime. The dotted line marks the $\mu = 1$ case where the two branches stay in NP for all g . The four black triangles on the μ axis marks the selected μ for generating the plots in Fig. 2. In **(b)** and **(c)** we plot $F_-(\bar{x})$ without ($\gamma_2 = 0$) and with ($\gamma_2 = 1$) nonlinear decay, respectively, in the inverted regime with $\mu = 2$ and different values of g . We have set $\gamma_1 = 1$.

tively. While the first-order boundary can only be obtained numerically (see Appendix A), the second-order boundary is determined analytically by $c_2^{\pm} = 0$, which yields a critical spin-boson coupling:

$$g_c = \sqrt{|1 + \gamma_1^2 - \mu^2| / |\mu - 1|}. \quad (5)$$

Some interesting conclusions can be drawn from Eq. (5): (1) When $\mu = 0$, g_c reduces to that of the open QRM with linear decay. As long as $\mu < 1$, the (+) branch is always in the NP, while the (-) branch is in NP when $g < g_c$ and in SRP when $g > g_c$, exhibiting a second-order DPT at $g = g_c$. (2) At $\mu = 1$ (vertical dotted line in Fig. 1(a)), we have $g_c \rightarrow \infty$ such that both branches remain in the NP for all g . The condition $\mu = 1$ coincides with the critical point for spectral collapse in a parametrically amplified oscillator [59]. (3) At $\mu = \mu_c \equiv \sqrt{1 + \gamma_1^2}$ (vertical dot-dashed line in Fig. 1(a)), we have $g_c = 0$. It is particularly interesting to note that, when $\mu > \mu_c$, the system enters the “inverted” regime, where the (+) branch always stays in SRP for any values of g , and the (-) branch is in SRP for $g < g_c$ and in NP for $g > g_c$. The plot of $F_-(\bar{x})$ in Fig. 1(b) and (c) provide an interpretation of the underlying physics. With $\mu > \mu_c$, the PA induces an anti-confining inverted harmonic potential, whereas the spin-boson coupling acts to restore local stability at $\bar{x} = 0$ (see more details in Appendix G). In Fig. 2, we plot the MF predictions of $\bar{n}_{ss}(g), s_z(g)$ for the branch that undergoes DPT in different regimes across the phase diagram.

Although The critical coupling g_c is independent of γ_2 ,

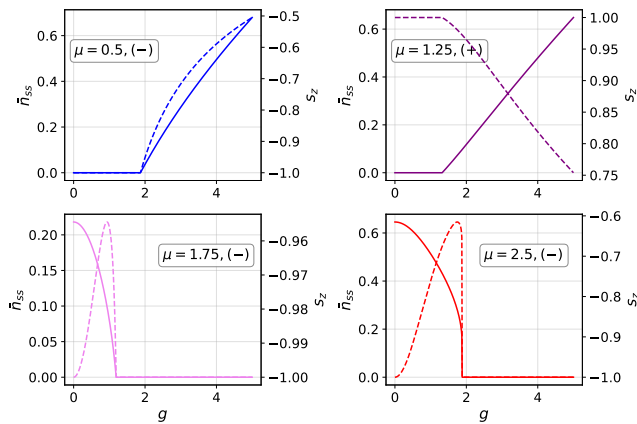


Figure 2: Mean-field predictions for the steady-state normalized boson number \bar{n}_{ss} (solid lines, left marker) and spin polarization s_z (dashed lines, right marker) as a function of g . The plots illustrate the specific branch undergoing DPT for selected values of μ (marked by black triangles on the μ axis of Fig. 1). Legends indicate the specific value of μ and the plotted branch. All other parameters are identical to those used in Fig. 1.

the two-photon decay plays a crucial role in our model. This can be immediately seen by comparing Fig. 1(b) and (c). First, the SRP in the inverted regime is stabilized by the nonlinear decay. Fig. 1(b) shows that F_- does not support stable minimum at $\bar{x} \neq 0$. By contrast, for finite γ_2 , as illustrated in Fig. 1(c), F_- does possess local minimums at $\bar{x} \neq 0$ when $g < g_c$. A similar stabilization effect has been observed in the two-photon Dicke model [53]. Second, the two-photon decay enables the tricritical behavior. To see this, we need to consider the c_4^\pm coefficient in $F_\pm(x)$:

$$c_4^\pm = \pm(\mu - 1)g^4/2 + \gamma_2\gamma_1(2\mu \pm g^2)/(\mu - 1). \quad (6)$$

Crucially, in the inverted regime, the sign of c_4^- can be tuned freely when $g = g_c$, indicating the existence of a TCP in the $(-)$ branch at $c_2^- = c_4^- = 0$. With fixed μ and γ_1 , the tricritical condition can be expressed in terms of a critical nonlinear dissipation rate:

$$\gamma_{2,c} = (\mu - 1)^2 g_c^4 / (2\gamma_1(2\mu - g_c^2)). \quad (7)$$

The DPT that occurs in the $(-)$ branch in the inverted regime is of first (second) order for $\gamma_2 < \gamma_{2,c}$ ($\gamma_2 > \gamma_{2,c}$).

Quantum formalism beyond mean-field – For realistic experimental and numerical simulations, η can only be tuned to a finitely large value. The MF approach then becomes insufficient because it neglects the mixing and the non-Gaussian features of the steady state by presuming a simple bosonic coherent state. Here we go beyond the MF by employing the adiabatic approximation: since the energy scale of the spin is much larger than the bosonic frequency, we treat $(a + a^\dagger) = \sqrt{2}x$ in the spin-boson interaction as a quasi-static coordinate and diagonalize H in the spin basis after a unitary transformation

$U_S = \exp[-i\sigma_y/2 \arctan(g(a + a^\dagger)/\sqrt{\eta})]$ [60, 61]. The purpose of the the unitary transformation is to decouple the spin and the bosons (see Appendix C). After projecting onto the adiabatic spin basis $|\pm\rangle$ (the eigenstates of $U_S^\dagger \sigma_z U_S$), we obtain a set of decoupled master equations:

$$\begin{aligned} \partial_t \rho_\pm &= -i[H_\pm, \rho_\pm] + 2\kappa_1 \mathcal{D}_a[\rho_\pm] + 2\kappa_2 \mathcal{D}_{a^2}[\rho_\pm], \\ H_\pm &= \omega_0 a^\dagger a + \frac{\mu}{2} \omega_0 (a^2 + a^{\dagger 2}) \pm V_{\text{nl}}(x), \end{aligned} \quad (8)$$

where ρ_\pm are the bosonic density matrices obtained by projecting $U_S^\dagger \rho U_S$ on $|\pm\rangle$ and we have defined a nonlinear potential:

$$V_{\text{nl}}(x) = (\omega_0 \eta / 2) \sqrt{2g^2 x^2 / \eta + 1}, \quad (9)$$

which exactly maps to the nonlinear force in the MF equation as $f_{\text{nl}} \propto -dV_{\text{nl}}/dx|_{x=\sqrt{\eta}\bar{x}}$, indicating that the adiabatic spin basis $|\pm\rangle$ corresponds to the (\pm) branches defined in the MF theory.

Since no coherent coupling exists between $|+\rangle$ and $|-\rangle$, the steady state in the adiabatic frame can be described by a classical mixture $\rho'_{ss} = p_+ \rho_{ss,+} |+\rangle\langle+| + p_- \rho_{ss,-} |-\rangle\langle-|$, where $\rho_{ss,\pm}$ are the bosonic steady states of Eq. (8). The weights p_\pm are determined by the off-diagonal components of the transformed jump operators in the $|\pm\rangle$ basis [35]. In Appendix D, we derive the expressions of p_\pm perturbatively.

In the inverted regime, the DPTs are confined to the $(-)$ branch. To accurately characterize critical behaviors, it is essential to isolate the $(-)$ branch. Experimentally, this can be achieved by a spin measurement in the adiabatic basis with post selection on $|-\rangle$. This requires an implementation of the unitary transformation U_{S_1} . In practice, this can be done by applying a position-dependent spin rotation $U_{S_1} = \exp(\frac{-ig}{2\sqrt{\eta}}(a + a^\dagger)\sigma_y)$ which approximates U_S (see Appendix E for numerical justification). Notably, U_{S_1} can be realized experimentally using the same techniques employed to generate the spin-boson interaction in the QRM. For the remainder of the work, we focus exclusively on the properties of the $(-)$ branch.

Semi-classical Langevin theory – To further understand the properties of $\rho_{ss,-}$ near the TCP, we analyze the system under the semi-classical limit, where η is large but the quantum phase coherence remains significant [62]. Applying the Keldysh formalism, we map the $(-)$ branch Master equation in (8) to a semi-classical Langevin equation by including leading-order quantum fluctuations [63]. In the regime of weak linear-dissipation ($\gamma_1 \ll |1 - \mu|$), the position variance dominates over the momentum variance ($\Delta x^2 \gg \Delta p^2$) and the steady-state Wigner function W_{ss}^- admits an approximate analytical solution which takes a Boltzmann form [49]:

$$W_{ss}^- = (1/Z_0) \exp[-(mv^2/2 + U(x))/T_{\text{eff}}]. \quad (10)$$

Here Z_0 is a normalization factor. We define the effective mass as $m = 1$ for convenience. With $v = -\omega_0(\mu - 1)p -$

Exponent	QRM* ($C_4 > 0$)	QRM* (TCP)	QRM/QDM(Closed)	QRM/QDM ($\kappa_2 = 0$)	Kerr/Amplified
ν	1	1	1/2	1	1
ζ	1/2	2/3	1/3	1/2	2/3
ξ	2	3/2	3/2	2	3/2

Table I: Critical and finite scaling exponents for different models. In each column we have included the critical exponent for order parameter (ν), the finite scaling exponent (ζ), and the coherent length exponent (ξ). From left to right we list the above exponents for the following models: the model studied in this paper (*) in the second-order DPT regime ($C_4 > 0$) and at the TCP ($C_4 = 0$), the closed QRM/QDM, the open QRM/QDM with single photon decay, and the resonant Kerr oscillator with single-photon decay/the parametrically amplified oscillator with two-photon decay.

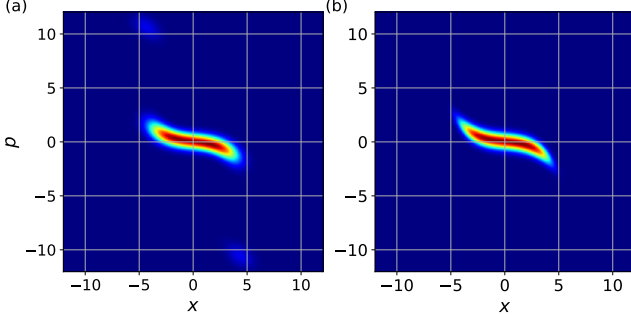


Figure 3: Wigner functions of the steady state at the TCP. (a). Steady-state wigner function of the complete model (Eq. (2)) calculated numerically. (b). Steady-state Wigner function of the (-) branch, evaluated using Eq. (10). Parameters: $\omega_0 = 1, \eta = 2500, g \sim 1.73, \gamma_1 = 0.1, \gamma_2 \sim 44.26$. The exact values of g, γ_2 are determined by the TCP conditions in Eqs. (5),(7).

$\kappa_1 x - \kappa_2 x^3$ and $T_{\text{eff}} = \frac{1}{4}(\mu - 1)^2$, the effective potential is given by:

$$U(x) = \frac{1}{2}\omega_0^2[(1 - \mu^2) + \gamma_1^2]x^2 + \frac{\omega_0^2}{2\eta}\gamma_1\gamma_2x^4 + \frac{1}{6}\frac{(\omega_0\gamma_2)^2}{\eta^2}x^6 + \omega_0(\mu - 1)V_{\text{nl}}(x) \quad (11)$$

where $V_{\text{nl}}(x)$ is the nonlinear potential in Eq. (9). Detailed derivation of W_{ss} starting from Eq. (8) is presented in Appendix F and the plots of $U(x)$ are given in Appendix G.

In Fig. 3 we benchmark Eq. (10) with respect to the steady-state Wigner function of the complete model (Eq. (2)), illustrating that W_{ss}^- successfully captures the structure of the (-) branch (pattern in the center) at the TCP[64]. The two dim off-center peaks in Fig 3(a) correspond to the (+) branch in the SRP. The relative weights of the two branches can be well explained by the formula of p_+/p_- derived in Appendix D. Notably, the overall distribution possesses central symmetry, as a result of the weak Z_2 symmetry in Eq. (2), enforcing $\langle a \rangle(t \rightarrow \infty) = 0$ at finite η . The mean-field prediction $\alpha_{\text{mf}} \neq 0$ is only valid in the $\eta \rightarrow \infty$ limit with Z_2 symmetry breaking

[11, 14].

Finite-size scaling and universality class – A hallmark of tricriticality is the existence of two universality classes, characterized by distinctive scaling laws [65, 66]. These scaling laws can be correctly predicted by tracking the effective potential $U(x)$ to the order of x^6 . Expanding V_{nl} to order (η^{-2}) gives:

$$U(x) \approx \sum_{k=1}^3 \frac{\omega_0^2}{2k} C_{2k} x^{2k}; \quad C_2 = -(\mu - 1)(g_c^2 - g^2), \quad (12)$$

$$C_4 = \frac{1}{\eta}(2\gamma_1\gamma_2 - (\mu - 1)g^4), \quad C_6 = \frac{1}{\eta^2}(\gamma_2^2 + 3(\mu - 1)g^6/2).$$

Note that the lower-order coefficients c_{2n} of $F(x)$ defined previously maps exactly to C_{2n} in the limit $|\mu - 1| \gg \gamma_1$. Since only the combined effects of PA (μ), two-photon dissipation (γ_2), and the QRM's intrinsic nonlinearity (g) can render C_2 and C_4 simultaneously tunable, their interplay is a necessary condition for the emergence of tricriticality in this model.

In the regime where Eq. (10) stays valid, we choose Δx^2 as the order parameter, as it effectively captures the bosonic fluctuations. To compute the critical exponent ν , we first assume $g_c \lesssim g$ but the difference $g^2 - g_c^2$ is still sufficiently large such that the x^2 term in $U(x)$ dominates. Integrating W_{ss} gives (see Appendix H):

$$\Delta x^2 \propto (g - g_c)^{-\nu} = (g - g_c)^{-1}, \quad (13)$$

The critical exponent $\nu = 1$ is identical to that of the open QRM and the Kerr oscillator with single-photon decay [16, 67].

Equation (13) is precise when $\eta \rightarrow \infty$. The frequency ratio η serves as an analog of the effective system size L in a spatially extended system, where the TDL is approached as $L \rightarrow \infty$. Consequently, we quantify finite-size effects by analyzing the finite-frequency scaling of the order parameter at the critical coupling ($g = g_c$) [68]. With large η and $C_4 > 0$, the x^4 term dominates in U , while the effect of the x^6 term can be observed at the TCP. Integrating W_{ss}^- in the above limits yields (see Appendix H):

$$\Delta x^2 \propto \eta^\zeta, \quad \zeta = \begin{cases} 1/2, & C_4 > 0 \text{ (second - order)} \\ 2/3, & C_4 = 0 \text{ (tricritical)} \end{cases} \quad (14)$$

We show the above scalings in Fig. 4 (a), where the numerical results are obtained by solving the steady state

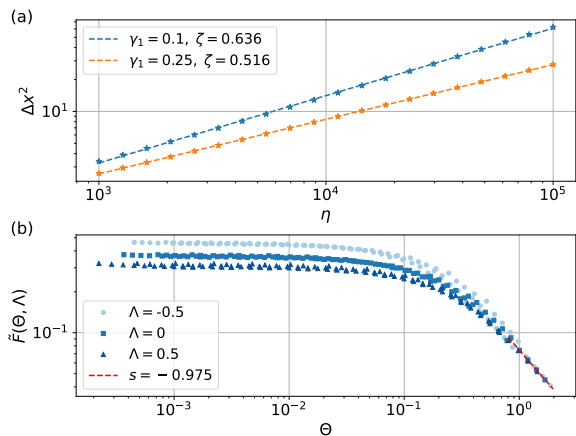


Figure 4: Verification of the finite-frequency scaling at critical point (Eq. (14)) and the generalized scaling ansatz (Eq. (15)). **(a)**. Δx^2 as a function of η at critical point $g = g_c$. The two values of γ_1 correspond to the second-order (orange) and tricritical (blue) DPTs. The dots represent numerical results and the dashed lines are linear fits in log-log scale, with the extracted slope (ζ_i) displayed in the labels. Parameters: $\omega_0 = 1, \mu = 2, \gamma_2 \sim 44.26$. **(b)**.

Normalized scaling ansatz \tilde{F} as a function of Θ . Data points of different shapes and colors show numerical results calculated for several fixed values of Λ . The red dashed line represents a linear fit in log-log space performed in the regime $\Theta > 0.8$, indicating the corresponding asymptotic power-law behavior described by Eq. (13). The numerical simulations use fixed parameters $\omega_0 = 1, \mu = 2, \gamma_1$ and samples from $\eta \in [10^4, 10^5]$, $(g - g_c) \in [10^{-5}, 10^{-2}]$. The value of γ_2 is determined accordingly such that Λ equals to the target fixed value.

of the $(-)$ branch decoupled Master equation in (8) [69]. The corresponding coherence length exponents can be obtained as $\xi = 2$ for $C_4 > 0$ and $\xi = 3/2$ for $C_4 = 0$ [70]. We summarize in Table I these exponents along those for several different models. Near the critical point, the finite-size crossover behaviors of the order parameter can be effectively captured by a scaling ansatz of the form (see Appendix H):

$$\Delta x^2 = L^{2/3} \tilde{F}(\Theta, \Lambda), \quad (15)$$

where $L = C_6^{-1/2} \propto \eta$, $\Theta = |g - g_c| L^{2/3}$, $\Lambda = C_4 L^{4/3}$.

As an illustrative example, we extract the function $\tilde{F}(\Theta, \Lambda)$ numerically in the inverted regime. We sample a set of $\{\eta, g\}$ near the critical point (g_c) for fixed γ_1, μ, Λ and solve for γ_2 that satisfies the defining equation of Λ . We numerically evaluate Θ and the corresponding value of $\Delta x^2 L^{-2/3}$ using the decoupled master equation (8). The results are presented in Fig. 4. For each fixed value of Θ , the collapse of all data points to an approximate single curve validates the ansatz in Eq. (15). \tilde{F} approaches a Λ -dependent constant as $\Theta \rightarrow 0$, while for large Θ it scales as $\tilde{F} \sim \Theta^{-1}$ and becomes independent of Λ . These limiting behaviors are consistent with asymp-

otic scalings in Eqs. (13), (14).

Conclusion – We have studied the superradiant DPT in a parametrically amplified open QRM with both single- and two-photon decay. Our MF analysis outlined four phases based on distinct steady states of the two spin branches. We locate an inverted regime where, contrary to conventional models exhibiting superradiance phase transition, the SRP (NP) emerges for weak (strong) spin-boson coupling. The inverted regime also supports a TCP. An adiabatic treatment followed by the semi-classical Langevin approach further captures the classical mixing and the non-Gaussian structures of the steady state beyond the mean field, demonstrating that the tricriticality arises from the intrinsic nonlinearity of the QRM, activated by the coherent and dissipative two-photon processes. The approximate analytical solution correctly predicts the two universality classes related to the TCP as well as the finite-size crossover behaviors. Our findings demonstrate the crucial role played by the controlled nonlinear dissipation in noisy light-atom interacting systems. The intrinsic nonlinearity in the QRM revealed by our analysis opens a pathway to higher-order criticality. The infinite order expansion of V_{nl} implies multicritical points maybe accessible through tailored interaction engineering (see Appendix I for a brief discussion). Exploring these exotic regimes represents a compelling direction for future research.

The authors acknowledge Yilun Xu for his valuable advice. We also thank Diego Fallas Padilla and Lin Jiao for insightful discussions. This work is supported by the NSF (Grant No. PHY-2513089) and the Welch Foundation (Grant No. C-1669).

* mz40@rice.edu

† hpu@rice.edu

- [1] I. I. Rabi. *Space Quantization in a Gyration Magnetic Field*. Phys. Rev. **51**, 652–654 (1937).
- [2] D. Braak. *Integrability of the Rabi Model*. Phys. Rev. Lett. **107**, 100401 (2011).
- [3] Q. Xie, H. Zhong, M. T. Batchelor, and C. Lee. *The quantum Rabi model: solution and dynamics*. Journal of Physics A: Mathematical and Theoretical **50**, 113001 (2017).
- [4] Y. K. Wang and F. T. Hioe. *Phase Transition in the Dicke Model of Superradiance*. Phys. Rev. A **7**, 831–836 (1973).
- [5] M.-J. Hwang, R. Puebla, and M. B. Plenio. *Quantum Phase Transition and Universal Dynamics in the Rabi Model*. Phys. Rev. Lett. **115**, 180404 (2015).
- [6] S. Chakravarty. *Quantum Fluctuations in the Tunneling between Superconductors*. Phys. Rev. Lett. **49**, 681–684 (1982).
- [7] P. Werner, K. Völker, M. Troyer, and S. Chakravarty. *Phase Diagram and Critical Exponents of a Dissipative Ising Spin Chain in a Transverse Magnetic Field*. Phys. Rev. Lett. **94**, 047201 (2005).

- [8] E. M. Kessler, G. Giedke, A. Imamoglu, S. F. Yelin, M. D. Lukin, and J. I. Cirac. *Dissipative phase transition in a central spin system*. Phys. Rev. A **86**, 012116 (2012).
- [9] W. Casteels, R. Fazio, and C. Ciuti. *Critical dynamical properties of a first-order dissipative phase transition*. Phys. Rev. A **95**, 012128 (2017).
- [10] L. M. Sieberer, M. Buchhold, J. Marino, and S. Diehl. *Universality in driven open quantum matter*. Rev. Mod. Phys. **97**, 025004 (2025).
- [11] F. Minganti, A. Biella, N. Bartolo, and C. Ciuti. *Spectral theory of Liouvilans for dissipative phase transitions*. Phys. Rev. A **98**, 042118 (2018).
- [12] S. Fernández-Lorenzo and D. Porrás. *Quantum sensing close to a dissipative phase transition: Symmetry breaking and criticality as metrological resources*. Phys. Rev. A **96**, 013817 (2017).
- [13] S. Sur, Y. Wang, M. Mahankali, S. Paschen, and Q. Si. *Amplified response of cavity-coupled quantum-critical systems*. arXiv.2509.26620 (2025).
- [14] S. Lieu, R. Belyansky, J. T. Young, R. Lundgren, V. V. Albert, and A. V. Gorshkov. *Symmetry Breaking and Error Correction in Open Quantum Systems*. Phys. Rev. Lett. **125**, 240405 (2020).
- [15] Y.-J. Liu and S. Lieu. *Dissipative phase transitions and passive error correction*. Phys. Rev. A **109**, 022422 (2024).
- [16] M.-J. Hwang, P. Rabl, and M. B. Plenio. *Dissipative phase transition in the open quantum Rabi model*. Phys. Rev. A **97**, 013825 (2018).
- [17] F. Dimer, B. Estienne, A. S. Parkins, and H. J. Carmichael. *Proposed realization of the Dicke-model quantum phase transition in an optical cavity QED system*. Phys. Rev. A **75**, 013804 (2007).
- [18] J. Klinder, H. Keßler, M. Wolke, L. Mathey, and A. Hemmerich. *Dynamical phase transition in the open Dicke model*. Proceedings of the National Academy of Sciences **112**, 3290–3295 (2015).
- [19] Z. Zhiqiang, C. H. Lee, R. Kumar, K. J. Arnold, S. J. Masson, A. S. Parkins, and M. D. Barrett. *Nonequilibrium phase transition in a spin-1 Dicke model*. Optica **4**, 424–429 (2017).
- [20] Z. Zhang, C. H. Lee, R. Kumar, K. J. Arnold, S. J. Masson, A. L. Grimsmo, A. S. Parkins, and M. D. Barrett. *Dicke-model simulation via cavity-assisted Raman transitions*. Phys. Rev. A **97**, 043858 (2018).
- [21] X. Chen, Z. Wu, M. Jiang, X.-Y. Lü, X. Peng, and J. Du. *Experimental quantum simulation of superradiant phase transition beyond no-go theorem via antisqueezing*. Nature Communications **12** (2021).
- [22] W. Ning, R.-H. Zheng, J.-H. Lü, K. Chen, X. Zhu, F. Wu, Z.-B. Yang, and S.-B. Zheng. *Observation of photonic dynamics in dissipative quantum Rabi models*. APL Quantum **2**, 026137 (2025).
- [23] Z. Wu, C. Hu, T. Wang, Y. Chen, Y. Li, L. Zhao, X.-Y. Lü, and X. Peng. *Experimental Quantum Simulation of Multicriticality in Closed and Open Rabi Model*. Phys. Rev. Lett. **133**, 173602 (2024).
- [24] Y. Xu and H. Pu. *Emergent Universality in a Quantum Tricritical Dicke Model*. Phys. Rev. Lett. **122**, 193201 (2019).
- [25] G. Lyu, K. Kottmann, M. B. Plenio, and M.-J. Hwang. *Multicritical dissipative phase transitions in the anisotropic open quantum Rabi model*. Phys. Rev. Res. **6**, 033075 (2024).
- [26] X.-Q. Zhao, N. Liu, and J.-Q. Liang. *First-Order Quantum Phase Transition for Dicke Model Induced by Atom-Atom Interaction**. Communications in Theoretical Physics **67**, 511 (2017).
- [27] J. Yang, Z. Shi, Z.-B. Yang, L.-t. Shen, and S.-B. Zheng. *First-order quantum phase transition in the squeezed Rabi model*. Physica Scripta **98**, 045107 (2023).
- [28] Y.-Q. Lu and Y.-Y. Zhang. *Quantum tricriticality in a generalized quantum Rabi system*. New Journal of Physics **26**, 063010 (2024).
- [29] Y.-Z. Wang, T. Ye, and Q.-H. Chen. *Quantum tricritical point induced by staggered qubit biases in a two-qubit quantum Rabi model*. Communications in Theoretical Physics **77**, 125702 (2025).
- [30] A. Azizi and R. Nessler. *The Kerr-Induced Superradiant Tricritical Point*. arXiv.2509.04530 (2025).
- [31] D. Fallas Padilla and H. Pu. *Tricritical Dicke model with and without dissipation*. Phys. Rev. A **108**, 033706 (2023).
- [32] C. J. Zhu, L. L. Ping, Y. P. Yang, and G. S. Agarwal. *Squeezed Light Induced Symmetry Breaking Superradiant Phase Transition*. Phys. Rev. Lett. **124**, 073602 (2020).
- [33] B. Debecker, J. Martin, and F. m. c. Damanet. *Controlling Matter Phases beyond Markov*. Phys. Rev. Lett. **133**, 140403 (2024).
- [34] Z. Zhang, Q. Miao, and G. S. Agarwal. *Time crystals and nonequilibrium dissipative phase transitions mediated by squeezed bath*. Phys. Rev. A **112**, 033708 (2025).
- [35] M. Kang, Y. Zhang, K. R. Brown, and T. Barthel. *Non-Gaussian Phase Transition and Cascade of Instabilities in the Dissipative Quantum Rabi Model*. arXiv.2507.07092 (2026).
- [36] D. Kienzler, H.-Y. Lo, B. Keitch, L. de Clercq, F. Lepold, F. Lindenfesler, M. Marinelli, V. Negnevitsky, and J. P. Home. *Quantum harmonic oscillator state synthesis by reservoir engineering*. Science **347**, 53–56 (2015).
- [37] A. Chenu, M. Beau, J. Cao, and A. del Campo. *Quantum Simulation of Generic Many-Body Open System Dynamics Using Classical Noise*. Phys. Rev. Lett. **118**, 140403 (2017).
- [38] F. Petziol and A. Eckardt. *Cavity-Based Reservoir Engineering for Floquet-Engineered Superconducting Circuits*. Phys. Rev. Lett. **129**, 233601 (2022).
- [39] V. So, M. Duraisamy Suganthi, M. Zhu, A. Menon, G. Tomaras, R. Zhuravel, H. Pu, P. G. Wolynes, J. N. Onuchic, and G. Pagano. *Quantum simulation of charge and exciton transfer in multi-mode models using engineered reservoirs*. Nature Communications (2025).
- [40] K. Sun, M. Kang, H. Nuomin, G. Schwartz, D. N. Beratan, K. R. Brown, and J. Kim. *Quantum simulation of spin-boson models with structured bath*. Nature Communications **16** (2025).
- [41] Y. Li, Y. Li, X. Cheng, L. Wang, X. Zhao, W. Hou, K. Rehan, M. Zhu, L. Yan, X. Qin, X. Peng, H. Yuan, Y. Lin, and J. Du. *Programmable multi-mode entanglement via dissipative engineering in vibrating trapped ions*. Science Advances **11**, eadv7838 (2025).
- [42] V. So, M. Zhu, M. D. Suganthi, A. Menon, G. Tomaras, R. Zhuravel, H. Pu, and G. Pagano. *Experimental Realization of Thermal Reservoirs with Tunable Temperature in a Trapped-Ion Spin-Boson Simulator*. arXiv.2511.08689 (2025).
- [43] J. M. T. Thompson and H. B. Stewart. *Nonlinear dynamics and chaos*. John Wiley & Sons (2002).

- [44] T. E. Lee and H. R. Sadeghpour. *Quantum Synchronization of Quantum van der Pol Oscillators with Trapped Ions*. Phys. Rev. Lett. **111**, 234101 (2013).
- [45] Z. Leghtas, S. Touzard, I. M. Pop, A. Kou, B. Vlastakis, A. Petrenko, K. M. Sliwa, A. Narla, S. Shankar, M. J. Hatridge, M. Reagor, L. Frunzio, R. J. Schoelkopf, M. Mirrahimi, and M. H. Devoret. *Confining the state of light to a quantum manifold by engineered two-photon loss*. Science **347**, 853–857 (2015).
- [46] Y. Li, Z. Xie, X. Yang, Y. Li, X. Zhao, X. Cheng, X. Peng, J. Li, E. Lutz, Y. Lin, and J. Du. *Experimental realization and synchronization of a quantum van der Pol oscillator*. Science Advances **11**, eady5649 (2025).
- [47] G. Beaulieu, F. Minganti, S. Frasca, V. Savona, S. Felicetti, R. Di Candia, and P. Scarlino. *Observation of first- and second-order dissipative phase transitions in a two-photon driven Kerr resonator*. Nature Communications **16** (2025).
- [48] C. Berdou, A. Murani, U. Réglade, W. Smith, M. Villiers, J. Palomo, M. Rosticher, A. Denis, P. Morfin, M. Delbecq, T. Kontos, N. Pankratova, F. Rautschke, T. Perronnin, L.-A. Sellem, P. Rouchon, A. Sarlette, M. Mirrahimi, P. Campagne-Ibarcq, S. Jezouin, R. Lescanne, and Z. Leghtas. *One Hundred Second Bit-Flip Time in a Two-Photon Dissipative Oscillator*. PRX Quantum **4**, 020350 (2023).
- [49] V. Y. Mylnikov, S. O. Potashin, G. S. Sokolovskii, and N. S. Averkiev. *Emergent equilibrium and quantum criticality in a two-photon dissipative oscillator*. Phys. Rev. Res. **7**, 013061 (2025).
- [50] N. Bartolo, F. Minganti, W. Casteels, and C. Ciuti. *Exact steady state of a Kerr resonator with one- and two-photon driving and dissipation: Controllable Wigner-function multimodality and dissipative phase transitions*. Phys. Rev. A **94**, 033841 (2016).
- [51] M. Malekakhlagh and A. W. Rodriguez. *Quantum Rabi Model with Two-Photon Relaxation*. Phys. Rev. Lett. **122**, 043601 (2019).
- [52] H. Li, J.-K. Shi, L.-B. Fan, Z.-M. Li, and C.-C. Shu. *Anisotropic Rabi model with two-photon relaxation*. Phys. Rev. A **110**, 023708 (2024).
- [53] A. Jayesh Shah, P. Kirton, S. Felicetti, and H. Alaëian. *Dissipative Phase Transition in the Two-Photon Dicke Model*. Phys. Rev. Lett. **135**, 173602 (2025).
- [54] M. J. Collett and C. W. Gardiner. *Squeezing of intracavity and traveling-wave light fields produced in parametric amplification*. Phys. Rev. A **30**, 1386–1391 (1984).
- [55] L.-A. Wu, H. J. Kimble, J. L. Hall, and H. Wu. *Generation of Squeezed States by Parametric Down Conversion*. Phys. Rev. Lett. **57**, 2520–2523 (1986).
- [56] W. Ge, B. C. Sawyer, J. W. Britton, K. Jacobs, J. J. Bollinger, and M. Foss-Feig. *Trapped Ion Quantum Information Processing with Squeezed Phonons*. Phys. Rev. Lett. **122**, 030501 (2019).
- [57] H.-P. Breuer and F. Petruccione. *The theory of open quantum systems*. OUP Oxford (2002).
- [58] Y. Xu, F.-X. Sun, W. Zhang, Q. He, and H. Pu. *Phase Transition and Multistability in Dicke Dimer*. Phys. Rev. Lett. **133**, 233604 (2024).
- [59] C. A. Downing and A. Vidiella-Barranco. *Parametrically driving a quantum oscillator into exceptionality*. Scientific Reports **13** (2023).
- [60] S. Ashhab and F. Nori. *Qubit-oscillator systems in the ultrastrong-coupling regime and their potential for preparing nonclassical states*. Phys. Rev. A **81**, 042311 (2010).
- [61] J. Larson and E. K. Irish. *Some remarks on ‘superradiant’ phase transitions in light-matter systems*. Journal of Physics A: Mathematical and Theoretical **50**, 174002 (2017).
- [62] L. M. Sieberer, M. Buchhold, and S. Diehl. *Keldysh field theory for driven open quantum systems*. Reports on Progress in Physics **79**, 096001 (2016).
- [63] E. G. D. Torre, S. Diehl, M. D. Lukin, S. Sachdev, and P. Strack. *Keldysh approach for nonequilibrium phase transitions in quantum optics: Beyond the Dicke model in optical cavities*. Phys. Rev. A **87**, 023831 (2013).
- [64] J. Johansson, P. Nation, and F. Nori. *QuTiP: An open-source Python framework for the dynamics of open quantum systems*. Computer Physics Communications **183**, 1760–1772 (2012). The numerical steady-state solutions of Lindbladian master equations in this paper are obtained using the direct LU factorization provided by the open source package QuTiP. For each solution we choose the boson truncation level n_c such that truncation error $\text{tr}(\rho_{ss}|n_c - 1\rangle\langle n_c - 1|) < 10^{-8}$.
- [65] H. Nishimori and G. Ortiz. *Elements of phase transitions and critical phenomena*. Oup Oxford (2010).
- [66] N. Goldenfeld. *Lectures on phase transitions and the renormalization group*. CRC Press (2018).
- [67] X. H. H. Zhang and H. U. Baranger. *Driven-dissipative phase transition in a Kerr oscillator: From semiclassical \mathcal{PT} symmetry to quantum fluctuations*. Phys. Rev. A **103**, 033711 (2021).
- [68] V. Ardourel and S. Bangu. *Finite-size scaling theory: Quantitative and qualitative approaches to critical phenomena*. Studies in History and Philosophy of Science **100**, 99–106 (2023).
- [69] (). At large η , solving the complete model in Eq.(8) requires a huge bosonic truncation level and can be resource-consuming because the (+) is always in the SRP. We solve the decoupled master equation for (−) branch instead to access the results at large η . In principle, these results can be obtained by applying the rotation-measurement scheme mentioned previously.
- [70] R. Botet, R. Jullien, and P. Pfeuty. *Size Scaling for Infinitely Coordinated Systems*. Phys. Rev. Lett. **49**, 478–481 (1982).
- [71] (). In principle a better consistency can be observed at larger η . However, since the (+) branch is in the SRP, further increasing η will cost huge computational resources.
- [72] Y. Zhang and T. Barthel. *Criteria for Davies irreducibility of Markovian quantum dynamics*. Journal of Physics A: Mathematical and Theoretical **57**, 115301 (2024).
- [73] H. J. Carmichael. *Statistical methods in quantum optics 1: master equations and Fokker-Planck equations*. Springer Science & Business Media (2013).
- [74] C. W. Gardiner et al. *Handbook of stochastic methods*, Volume 3. springer Berlin (2004).
- [75] M. E. Fisher and M. N. Barber. *Scaling Theory for Finite-Size Effects in the Critical Region*. Phys. Rev. Lett. **28**, 1516–1519 (1972).
- [76] K. Binder, D. W. Heermann, and K. Binder. *Monte Carlo simulation in statistical physics*, Volume 8. Springer (1992).

APPENDIX

Appendix A: Determination of critical conditions using the Landau theory

Following the definitions of \bar{x}, \bar{p} in the main text and $s_i = \langle \sigma_i \rangle$, the corresponding Heisenberg equations in the thermodynamical limit (TDL) are given by:

$$\begin{aligned} \partial_t \bar{x} &= \omega_0 [(1 - \mu) \bar{p} - \gamma_1 \bar{x} - \gamma_2 (\bar{x}^2 + \bar{p}^2) \bar{x}], \\ \partial_t \bar{p} &= \omega_0 [- (1 + \mu) \bar{x} - \frac{g}{\sqrt{2}} s_x - \gamma_1 \bar{p} - \gamma_2 (\bar{x}^2 + \bar{p}^2) \bar{p}], \\ \partial_t s_x &= -\Omega s_y, \quad \partial_t s_z = \Omega \sqrt{2} g \bar{x} s_y, \\ \partial_t s_y &= \Omega (s_x - \sqrt{2} g \bar{x} s_z), \end{aligned} \quad (\text{A1})$$

Setting the LHS to 0 we obtain the fixed point equations:

$$\begin{aligned} 0 &= \sqrt{2} g s_+ + \bar{x} + \gamma_1 \bar{p} + \mu \bar{x} + \gamma_2 \bar{p} (\bar{x}^2 + \bar{p}^2), \\ 0 &= (1 - \mu) \bar{p} - \gamma_1 \bar{x} - \gamma_2 \bar{x} (\bar{x}^2 + \bar{p}^2), \\ 0 &= -\sqrt{2} s_+ + g \bar{x} s_z \\ 1 &= 4s_+^2 + s_z^2, \end{aligned} \quad (\text{A2})$$

where we have introduced $s_+ = \langle \sigma_+ \rangle$ and replaced the s_z equation with the spin conservation identity. Solving the last two equations for s_+ in terms of \bar{x} and substituting back to the first equation results in the nonlinear effective force $f_{\text{nl}}(x) = g^2 x (2g^2 x^2 + 1)^{-1/2}$. The \bar{x}, \bar{p} equations can then be combined into a compact form that only involves the variable $u_x = \bar{x}^2$:

$$\begin{aligned} h(u_x) &= u_x (\gamma_1 + \gamma_2 (u_p + u_x))^2 - (1 - \mu)^2 u_p = 0, \\ u_p &= \frac{1}{1 - \mu} u_x [- (1 + \mu) \mp g^2 (2g^2 u_x + 1)^{-1/2}], \end{aligned} \quad (\text{A3})$$

where we have introduced the variable $u_p = \bar{p}^2$. We note that the $+, -$ signs in u_p arise from the fact that $s_z = \pm (2g^2 u_x + 1)^{-1/2}$ can take both positive/negative values, which corresponds to the two spin branches $(+, -)$ as mentioned in the main text.

To the function $F(x)$ in the main text, we expand the nonlinear factor $(2gu_x + 1)^{-1/2}$ in f_{nl} into a power series $G(u_x) = \sum_{n=0}^N b_n u_x^n$, or expanding $f_{\text{nl}}(x)$ to the order of x^{2N+1} equivalently. Since we focus on non-trivial solutions, u_x^1 can be canceled out from Eq. (A3), such that the RHS becomes a polynomial of u_x of the order $2N + 2$. Integrating $h(u_x)/u_x$ and replacing u_x by x^2 results in $F_{\pm}(x) = \sum_{n=0}^{2N+3} c_{2n}^{\pm} x^{2n}$ in the main text such that $h(u_x) = 0$ is equivalent to $dF_{\pm}(x)/dx = 0$. Though $N \rightarrow \infty$ is required to precisely describe the solutions of Eq. (A3), for the purpose of studying tricriticality, it is sufficient to track c_2^{\pm}, c_4^{\pm} , whose exact forms (Eq. (4), (6) in the main text) can be straightforwardly obtained by expanding $F(x)$ to the order of $N = 1$ ($G(u_x) \rightarrow 1 - g^2 u_x$). The expansion remains a

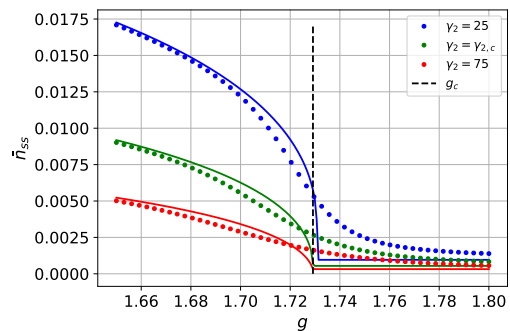


Figure 5: Normalized order parameter \bar{n}_{ss} as a function of g for different γ_2 . Dots represent the numerical solutions of the complete model (steady state of Eq. (2) of the main text) while dashed lines show mean-field predictions incorporating the classical mixture ansatz (see Appendix D). Colors denote the nature of the DPT: first-order (blue), tricritical (green), and second-order (red). The black dashed line marks the critical coupling for the second-order DPT. The deviation from MF predictions near the critical point demonstrates finite-size effects[71]. The parameters used for simulations are: $\omega_0 = 1, \eta = 2500, \mu = 2, \gamma_1 = 0.1$. and the corresponding $\gamma_{2,c} \sim 44.26$.

fairly good approximation when $g^2 u_x \ll 1$, which is valid near the critical point for a second-order DPT. For the first-order DPT in the system, this condition is usually satisfied when $1 \lesssim \gamma_2$ suggested by numerical results.

To obtain the conditions for the emergence of non-trivial solutions, we consider the exact equation $\tilde{f}(u_x) = H(u_x)/u_x = 0$. Since $\tilde{f}(u_x) \rightarrow \infty$ as $u_x \rightarrow \infty$ (assuming $\gamma_2 > 0$), if $\tilde{f}(0) = c_2^{\pm} < 0$, there is at least one solution $u_x > 0$ with $\tilde{f}'(u_x) > 0$ (stable non-trivial solution). Hence, $c_2^{\pm} < 0$ is a sufficient condition for the emergence of the SRP. However, $c_2^{\pm} = 0$ cannot be used as the exact critical condition for DPT, since a first-order DPT can happen when a non-trivial x emerges as a global minimum of $F(x)$, although $F(0)$ remains as a stable local minimum simultaneously, which is a common case in a Landau ϕ^6 theory. In our model, due to the nonlinearity, the exact critical condition can only be obtained numerically.

In Fig. 5, we show the transition from first- to second-order DPT across the TCP by plotting the order parameter \bar{n}_{ss} as a function of g for different nonlinear dissipation strength γ_2 , demonstrating a good consistency between MF and numerical results at large η .

Appendix B: Stabilization effect of two-photon dissipation

The nonlinear dissipation guarantees the existence of a stable fixed point by enforcing $\lim_{u_x \rightarrow \infty} \tilde{f}(u_x) \rightarrow \infty$. This stabilization is specifically important for the inverted regime ($\mu > \mu_c = \sqrt{1 + \gamma_1^2}$) as $\lim_{u_x \rightarrow \infty} \tilde{f}(u_x) \rightarrow$

$1 + \gamma_1^2 - \mu^2 < 0$ for $\gamma_2 = 0$ and it can be further demonstrated that no stable non-trivial fixed point exists without the two-photon decay.

When $\gamma_2 = 0$ the steady-state equation (A2) yields only the unstable trivial solution $\bar{x} = \bar{p} = 0$ for the (+) branch, indicating that both the NP and the SRP are unstable. For the (-) branch, when $g < g_c$ non-trivial solution does not exist, which is very different from the $\gamma_2 > 0$ case where superradiance emerges for $g < g_c$. A closed form non-trivial solution exists for $g > g_c$:

$$\begin{aligned} s_z &= \frac{1 + \gamma_1^2 - \mu^2}{g^2(\mu - 1)} = -\frac{g_c^2}{g^2}, \quad \bar{x} = -\frac{1}{\sqrt{2}g} \sqrt{1/s_z^2 - 1}, \\ s_+ &= \frac{1}{\sqrt{2}} g \bar{x} s_z, \quad \bar{p} = \frac{\gamma_1}{1 - \mu} \bar{x}. \end{aligned} \quad (\text{B1})$$

However, this solution is not stable, which can be verified by a linear stability analysis. Starting from Eq.(3) in the main text, we substitute $s_z = -\sqrt{1 - s_x^2 - s_y^2}$ such that the remaining equations become independent. We then compute the determinant of the corresponding Jacobi matrix at the fixed point given by Eq. (B1):

$$\det[J] = (\gamma_1^2 + 1 - \mu^2) \frac{1}{s_z} (s_z + \frac{1}{s_z}). \quad (\text{B2})$$

Since $s_z < 0$, $\gamma_1^2 + 1 - \mu^2 < 0$, $\det[J] < 0$, this solution is always unstable. For the trivial solution, following a similar analysis one can show that the related stability condition is given by $c_2^- > 0$, where c_2^- is defined in Eq. (4) in the main text. In the inverted regime this simplifies to $g > g_c$, which means the NP is always stable even without the two-photon decay.

Appendix C: Derivation of the decoupled bosonic master equations

We first derive the transformed Rabi Hamiltonian under the adiabatic approximation. The spin-dependent part of the Rabi Hamiltonian can be considered as a typical two-level system with effective detuning Ω and Rabi frequency $\lambda(a + a^\dagger)$, which can be diagonalized with a position-dependent rotation $U_S = \exp(-i\sigma_y/2 \arctan(g(a + a^\dagger)/\sqrt{\eta}))$. In the adiabatic basis the transformed Hamiltonian takes the form:

$$\begin{aligned} H_d &= U_S^\dagger H U_S = \sigma_z V_{\text{nl}}(x) + \omega_0 a^\dagger a + \frac{\mu}{2} \omega_0 (a^2 + a^{\dagger 2}), \\ V_{\text{nl}}(x) &= \frac{\omega_0 \eta}{2} \sqrt{2g^2 x^2 / \eta + 1}. \end{aligned} \quad (\text{C1})$$

where $x = (a + a^\dagger)/\sqrt{2}$. We have neglected the effects of U_S on the purely bosonic part $H_B = \omega_0 [a^\dagger a + \mu(a^2 + a^{\dagger 2})]$. The off-diagonal terms arising from $U_S^\dagger H_B U_S$ are at most of the order $o(\eta^0)$, which has a negligible effect compared to the dominant interaction term $V_{\text{nl}} \propto \eta^1$, since η is large. A series expansion of V_{nl} will reproduce

the Schrieffer-Wolff transformation derived in the SM of [5] up to arbitrary orders.

We then apply the transformation on both sides of the complete master equation (2) in the main text and evaluate $U_S^\dagger \mathcal{L}[\rho] U_S$. Projecting H_d on the adiabatic spin basis $|\pm\rangle$ leads to the coherent parts of (8). We now argue that the jump operators stay effectively invariant in the decoupled equations. Defining $\theta(x) = \arctan(gx/\sqrt{\eta/2})$ such that $U_S = \exp(-i\sigma_y \theta(x)/2)$ we have

$$\begin{aligned} c_1 = U_S^\dagger a U_S &= a + \frac{i}{\sqrt{2}} (U_S^\dagger [p, U_S]) = a + \frac{1}{\sqrt{2}} (U_S^\dagger \partial_x U_S) \\ &= a - i\epsilon(x) \sigma_y, \end{aligned} \quad (\text{C2})$$

where $\epsilon(x) = \frac{1}{2\sqrt{2}} \partial_x \theta(x)$, and

$$c_2 = U_S^\dagger a^2 U_S = a^2 - i(\epsilon(x)a + \epsilon(x)a) \sigma_y - \epsilon(x)^2. \quad (\text{C3})$$

Consider the transformed Lindbladian dissipator $\mathcal{D}_{c_i}[\rho]$. For c_1 , the correction $\epsilon(x) \sigma_y$ only generates off-diagonal effects through the quantum jump term $c_i \rho c_i^\dagger$ after projecting on $|\pm\rangle$. The correction term has a diagonal contribution of order $o(\eta)^{-1}$ through the anti-commutator $\{c_i^\dagger c_i, \rho\}$, as $\epsilon(x)$ is of order $o(\eta^{-1/2})$ in both NP and SRP. It can be safely neglected when η is large. Therefore, to the leading order $c_1 \sim a$ in the decoupled equation. A similar argument can be made in terms of projection and scaling to demonstrate that $c_2 \sim a^2$.

Appendix D: Perturbative calculation of the spin population

We aim to derive a perturbative solution for the spin weights p_\pm in the classical mixture ansatz $\rho'_{ss} = p_+ \rho_{ss,+} |+\rangle\langle+| + p_- \rho_{ss,-} |-\rangle\langle-|$. In the TDL, the effect of $\epsilon(x)$ can be completely neglected in the strict limit $\eta \rightarrow \infty$. Hence, the dynamics of the system can be exactly tracked by the decoupled bosonic master equation (8) in the main text, demonstrating the existence of a strong spin symmetry in the $|\pm\rangle$ basis as H, c_i all commutes with σ_z . The steady state is not unique and the weights p_+, p_- are determined by the initial condition[35, 72].

In the case where η is large but finite, the steady state becomes a unique mixed state. The spin-dependent part of the c_i generates non-trivial incoherent effects and they can no longer be neglected. The perturbative treatment performed to the order of $(x^2/\eta)^1$ in [35] shows that $p_+ = p_- = 0.5$ in the NP. We perform a similar calculation to track the steady state up to the order of $(x^2/\eta)^2$ by expanding the argument of U_S to the order of $(x/\sqrt{\eta})^5$. This expansion is valid when both branches are in the NP and remains accurate in the SRP when $\langle x \rangle^2 g^2 / \eta \ll 1$.

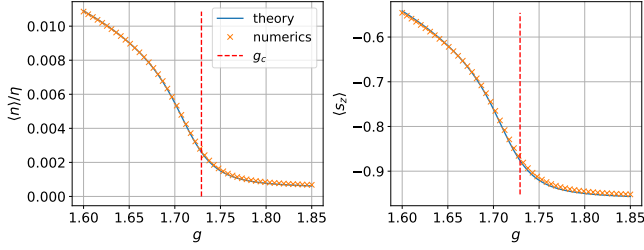


Figure 6: Verification of the approximate spin population relation in Eq. (D4). The dots show the steady-state expectation values of n, s_z obtained by numerically solving the complete model. The solid line plots the prediction of the perturbative formalism, which is obtained by first solving the decoupled master equations corresponding to Eq. (D1) numerically and then evaluating mixed state expectation values using Eq. (D4). The parameters used for simulation are $\eta = 2500, \gamma_1 = 0.1, \omega_0 = 1, \mu = 2$. γ_2 is set to the TCP point value ~ 44.25 . The fock space cutoff n_c is chosen for each g such that $\max(\text{tr}(\rho_{ss,n}|n_c - 1\rangle\langle n_c - 1|)) \sim 10^{-10}$.

The resulting decoupled master equation takes the form:

$$\begin{aligned} \partial_t \rho' &= \mathcal{L}'[\rho'] = -i[H', \rho'] + 2\kappa_1 \mathcal{D}_{c'_1}[\rho'] + 2\kappa_2 \mathcal{D}_{c'_2}[\rho'], \\ H' &= \frac{\Omega}{2} \sigma_z + \omega_0 a^\dagger a + \frac{\omega_0}{2} \mu (a^2 + a^{\dagger 2}) + \frac{\omega_0 g^2}{4} \sigma_z (a + a^\dagger)^2 \\ &\quad - \frac{\omega_0 g^4}{16\eta} \sigma_z (a + a^\dagger)^4 + \frac{\omega_0 g^6}{32\eta^2} \sigma_z (a + a^\dagger)^6. \end{aligned} \quad (\text{D1})$$

The relevant terms in the transformed jump operators are obtained by expanding $\epsilon(x)$ to the leading order:

$$c_1 \sim a - \frac{ig}{2\sqrt{\eta}} \sigma_y, \quad c_2 \sim a^2 - \frac{ig}{\sqrt{\eta}} \sigma_y a. \quad (\text{D2})$$

Projecting Eq. (D1) on $|\pm\rangle$ yields two decoupled master equations similar to those in (8) of the main text. We can approximate $\rho_{ss,\pm}$ with the steady state of these equations. In the steady state we require $\partial_t p_\pm = 0$, thus:

$$\partial_t \text{tr}(|+\rangle\langle +|\rho'_{ss}) = \text{tr}(|+\rangle\langle +|\mathcal{L}'[\rho'_{ss}]) = 0. \quad (\text{D3})$$

Explicitly evaluating (D3) gives the steady-state condition:

$$r_p = \frac{p_+}{p_-} = \frac{4\gamma_2 n_- / \eta + \gamma_1}{4\gamma_2 n_+ / \eta + \gamma_1}, \quad (\text{D4})$$

where $n_\pm = \text{tr}(a^\dagger a \rho_{ss,\pm})$.

We verify the above formalism by numerically solving the steady state of the complete model defined in Eq. (2) of the main text and then computing the corresponding photon number n and spin imbalance s_z . These expectations are compared to the mixed ansatz expectations evaluated from $\rho_{ss} = U_S \rho'_{ss} U_S^\dagger$, where ρ'_{ss} is constructed based on Eq. (D4). The results plotted in Fig. 6 demonstrate good agreement between the two methods. Eq. (D4) provides a straightforward explanation for the

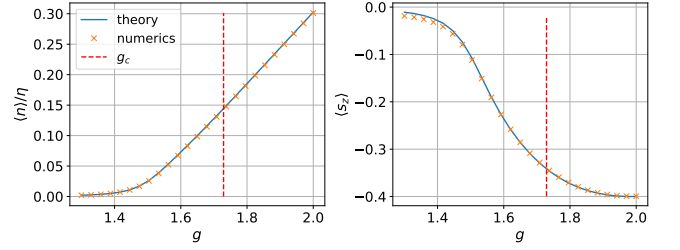


Figure 7: Verification of the complete spin population relation in Eq. (D5). The dots show the steady-state expectation values of n, s_z obtained by numerically solving the complete model. The solid line plots the prediction of the perturbative formalism, which is obtained by first solving the decoupled master equations corresponding to Eq. (8) in the main text numerically and then evaluating mixed state expectation values using Eq. (D5). The parameters used for simulation are $\eta = 250, \omega_0 = 1, \mu = 0, \gamma_1 = 1, \gamma_2 = 0.1$.

observation that the (+) branch component has a much smaller weight in the composite steady state Wigner function plotted in Fig. 3 of the main text, as compared to the (-) branch components. $\rho_{ss,+}$ is in the SRP which yields a much larger photon number compared to that of the $\rho_{ss,-}$ component near the TCP, leading to a small p_+/p_- predicted by the perturbative formalism.

The analytical formula above gives a clear and simple result, but breaks down in the regime $\langle x \rangle^2 g^2 / \eta \sim 1$. A typical example would be the behavior of the QRM with only linear decay ($\gamma_2 = 0$) as the system is tuned away from the critical point in the SRP. In this regime p_+/p_- decreases sharply as g increases, resulting in a steady state $\rho'_{ss} \rightarrow \rho_{ss,-}$. This contradicts the prediction of Eq. (D4) since n_+ remains as a small constant while n_- increases dramatically. The structure of ρ'_{ss} can be explained by a more precise treatment incorporating jump operators of the complete form derived in Eq. (C2),(C3). From the MF theory, a, a^\dagger can be taken as the order of $\sqrt{\eta}$, we then approximate $c_2 = a^2 - 2i\epsilon(x)a + o(\eta^{-1})$ in the SRP because $[\epsilon(x), a] \propto \partial_x \epsilon(x) \sim o(\eta^{-1})$. Following a similar approach as before, we derive a more accurate relation for the spin weights:

$$r_p = \frac{p_+}{p_-} = \frac{4\gamma_2 \langle O_2 \rangle_- / \eta + \gamma_1 \langle O_1 \rangle_-}{4\gamma_2 \langle O_2 \rangle_+ / \eta + \gamma_1 \langle O_1 \rangle_+}, \quad (\text{D5})$$

where $O_1 = \epsilon^2, O_2 = a^\dagger \epsilon^2 a$ and $\langle \dots \rangle_\pm$ stand for the expectation values taken with respect to $\rho_{ss,\pm}$, the steady states of the complete decoupled Master equation (8) of the main text. Eq. (D5) is a generalization of Eq. (D4). In Fig. 7 we numerically demonstrate that it correctly captures the steady state structure when the (-) branch is deep in the SRP.

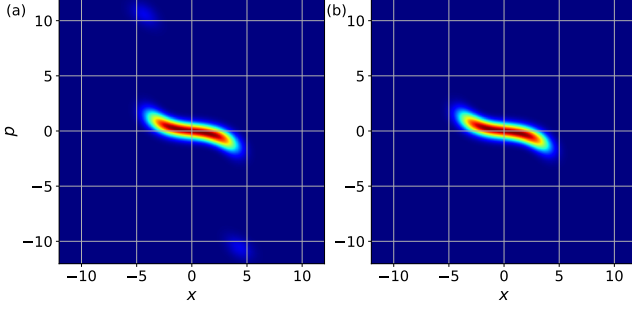


Figure 8: Wigner functions of the steady state at the TCP. (a). Steady-state wigner function of the complete model (Eq. (2)) calculated numerically. (b). Steady-state Wigner function of the $(-)$ branch, extracted using the U_{S_1} based rotation-measurement scheme. Parameters: $\omega_0 = 1$, $\eta = 2500$, $g \sim 1.73$, $\gamma_1 = 0.1$, $\gamma_2 \sim 44.26$. The exact values of g , γ_2 are determined by the TCP conditions in Eqs. (5),(7).

Appendix E: Isolating the spin branches

To isolate the spin branches, in principle, one needs to apply the complete spin rotation $U_S = \exp(-i\sigma_y/2 \arctan(g(a + a^\dagger)/\sqrt{\eta}))$, as derived in the previous section. However, this transformation is difficult to realize in actual experiments. When the system is in normal phase or near the critical point where $gx/\sqrt{\eta} \ll 1$, it is sufficient to expand the position-dependent rotation angle to the order of $1/\sqrt{\eta}$, resulting in an experimentally feasible rotation $U_{S_1} = \exp(\frac{-ig}{2\sqrt{\eta}}(a + a^\dagger)\sigma_y)$.

We verify the effectiveness of U_{S_1} numerically by applying the rotation-measurement scheme on the steady state ρ_{ss} of the complete model and compare the Wigner function of the extracted state with that of ρ_{ss} . The results plotted in Fig. 8 show that the U_{S_1} -based scheme successfully extracts the $(-)$ branch component from the steady-state mixture.

We further check if the scheme can reproduce observable values consistent with those obtained from the $(-)$ branch decoupled master equation by performing a similar set of numerical simulations as in Fig. 5. For fixed ω_0, μ, γ_1 and a chosen set of g, γ_2 , we first solve the complete model numerically (Eq. (2) in the main text) and calculate $n_{ss,-}$ using $\rho_{ss,-}$ extracted via U_{S_1} . In Fig. 9 we compare these results against those obtained by directly solving the decoupled master equation (Eq. (8) of the main text). The agreement between the two sets of datasets validates the U_{S_1} -based extraction scheme. This equivalence also provides us with a resource efficient method for simulating the critical behaviors of the $(-)$ branch near the TCP. By halving the effective Hilbert space, solving the steady state of the decoupled master equations requires only 1/4 of the memory compared to

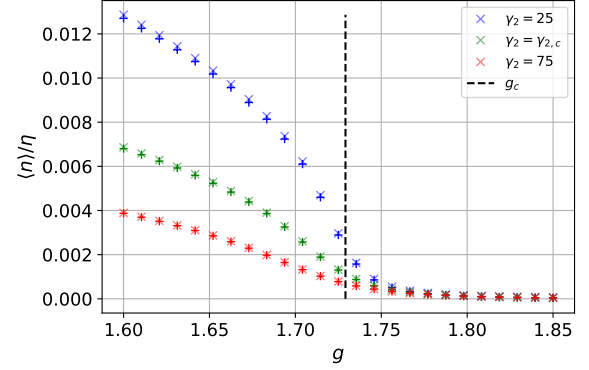


Figure 9: Normalized order parameter $\langle n \rangle / \eta$ as a function of g for different γ_2 obtained with two different methods. The "x" points of fainter colors represent the observable values extracted using the U_{S_1} -based scheme from the steady state of the complete model, while the "+" points correspond to those evaluated using the decoupled master equation. Different colors denote the nature of the DPT: first-order (blue), tricritical (green), and second-order (red). The black dashed line marks the critical coupling for the second-order DPT. The parameters used for simulations are: $\omega_0 = 1, \eta = 2500, \mu = 2, \gamma_1 = 0.1$, and the corresponding $\gamma_{2,c} \sim 44.26$.

solving the complete master equation. We leverage this computational advantage in the main text to access the large- η regime necessary for verifying the finite-frequency scaling laws.

Appendix F: Derivation of W_{ss} using the semi-classical Langevin theory

In this section we derive the approximated Wigner function W_{ss}^- in Eq. (10) of the main text. We focus on the $(-)$ branch while the $(+)$ branch result can be derived in a similar way. For convenience the \pm labels for the branches will be dropped. We start from the decoupled master equation (8) of the $(-)$ branch. The corresponding Keldysh action is given by:

$$\begin{aligned}
 S &= S_F + S_D + S_I \\
 S_F &= \int dt \alpha_+^* (i\partial_t - \omega_0) \alpha_+ - \alpha_-^* (i\partial_t - \omega_0) \alpha_- \\
 S_D &= -i\kappa_1 \int dt (\alpha_+ \alpha_-^* - \alpha_+^* \alpha_-) \\
 &\quad - i\kappa_2 \int dt (2\alpha_+^2 \alpha_-^{*2} - \alpha_+^{*2} \alpha_-^2 - \alpha_-^{*2} \alpha_+^2) \\
 S_I &= - \int dt (V_n^+ - V_n^-)
 \end{aligned} \tag{F1}$$

with $V_n^\pm = -\omega_0 \eta / 2 \sqrt{g^2 (\alpha_\pm + \alpha_\pm^*)^2 / \eta + 1}$ and α_+, α_- being the forward and backward fields, respectively. Performing the Keldysh rotation gives the action in terms of

classical and quantum fields $\alpha_{\pm} = (\alpha_c \pm \alpha_q)/\sqrt{2}$:

$$S = \int dt [\alpha_q^* (i\partial_t - \omega_0 + i\kappa_1) \alpha_c + \text{c.c.}] + S_I \\ + \int dt [2i\kappa_1 \alpha_q \alpha_q^* - \mu (\alpha_c \alpha_q + \alpha_c^* \alpha_q^*) + D_2] \\ D_2 = -i\kappa_2 (\alpha_c \alpha_q (\alpha_q^{*2} + \alpha_c^{*2}) - \alpha_c^* \alpha_q^* (\alpha_c^2 + 4\alpha_c \alpha_q + \alpha_q^2)). \quad (\text{F2})$$

We have kept the form of S_I unchanged as it requires special treatment in further derivations. We study fluctuations beyond mean-field by expanding the fields around the saddle point solution $\alpha_{c,q} = \alpha_{c,q0} + \delta\alpha_{c,q}$. Near the TCP we have $\alpha_{c,q0} \rightarrow 0$, the effective action S_c is obtained by replacing $\alpha_{c,q}$ with $\delta\alpha_{c,q}$. We then apply the semi-classical approximation by neglecting terms of higher than quadratic order in $\delta\alpha_q, \delta\alpha_q^*$, as they correspond to short-scale fluctuations [62]. For convenience, we henceforth use $\alpha_{c,q}$ to denote these fluctuations. Defining $x_{c,q} = (\alpha_{c,q} + \alpha_{c,q}^*)/\sqrt{2}$ we have

$$V_n^+ - V_n^- \\ = -\frac{\omega_0 \eta}{2} (\sqrt{g^2(x_c + x_q)^2/\eta + 1} - \sqrt{g^2(x_c - x_q)^2/\eta + 1}) \\ = -\sqrt{2} f(x_c) x_q + o(x_q^3), \quad f(x_c) = \frac{1}{\sqrt{2}} \frac{\omega_0 g^2}{\sqrt{g^2 x_c^2/\eta + 1}} x_c. \quad (\text{F3})$$

The partition function $Z = \int \mathcal{D}[\alpha_c, \alpha_q, \alpha_c^*, \alpha_q^*] e^{iS_c}$ is given by:

$$Z = \int \{ \mathcal{D}[\alpha_c, \alpha_q, \alpha_c^*, \alpha_q^*] \\ \times \exp(\int_t [(\partial_t - i\omega_0 + \kappa_1 + \kappa_2 |\alpha_c|^2) \alpha_c^* - i\mu \alpha_c + i f(x_c)] \alpha_q) \\ \times \exp(\int_t [(-\partial_t - i\omega_0 - \kappa_1 - \kappa_2 |\alpha_c|^2) \alpha_c - i\mu \alpha_c^* + i f(x_c)] \alpha_q^*) \\ \times \exp(\int_t -2(\kappa_1 + 2\kappa_2 |\alpha_c|^2) \alpha_q \alpha_q^*) \}. \quad (\text{F4})$$

The quadratic term $-2(\kappa_1 + 2\kappa_2 |\alpha_c|^2) \alpha_q \alpha_q^*$ in the exponential can be replaced by linear terms of α_q, α_q^* with the Hubbard-Stratonovich identity:

$$\exp(\int_t -\gamma \alpha_q \alpha_q^*) \\ = \int \mathcal{D}[\xi, \xi^*] \exp(\int_t [-\xi^* \xi - i\sqrt{\gamma} (\alpha_q^* \xi - \xi^* \alpha_q)]), \quad (\text{F5})$$

where ξ is a complex Gaussian white noise. Since κ_1 and κ_2 represent the rates of two independent dissipation channels, we apply the above identity to the corresponding terms separately by introducing two sets of stochastic variables ξ_1, ξ_2 . For the part with κ_2 , the linear term inside the exponential is given by $\phi_2 = -i2\sqrt{\kappa_2} |\alpha_c| (\alpha_q^* \xi_2 - \xi_2^* \alpha_q)$. We manually add a phase factor $\theta(t) = \arg(\alpha_c)$ into the noise and define $\xi_2' = \xi_2 e^{i\theta}$

such that $\phi_2 = -i2\sqrt{\kappa_2} (\alpha_c^* \alpha_q^* \xi_2' - \xi_2'^* \alpha_c \alpha_q)$. Here ξ_2' is also a Gaussian white noise given the property of ξ_2 . This transformation makes the resulting Langevin equation take the same form as the mean field equation when the stochastic noise terms are ignored. With the above transformations, we have:

$$Z = \int \{ \mathcal{D}[\alpha_c, \alpha_c^*, \xi_1, \xi_1^*, \xi_2, \xi_2^*] \exp(\int_t -(\xi_1^* \xi_1 + \xi_2^* \xi_2)) \\ \times \delta \left[(\partial_t - i\omega_0 + \kappa_1 + \kappa_2 |\alpha_c|^2) \alpha_c^* - i\mu \alpha_c + i f(x_c) + i\tilde{\xi}^* \right] \\ \times \delta \left[(-\partial_t - i\omega_0 - \kappa_1 - \kappa_2 |\alpha_c|^2) \alpha_c - i\mu \alpha_c^* + i f(x_c) - i\tilde{\xi} \right] \}, \\ \tilde{\xi} = \sqrt{2\kappa_1} \xi_1 + 2\sqrt{\kappa_2} \xi_2 \alpha_c^*, \quad (\text{F6})$$

which shows that the dynamics of the system can be described by the Langevin equation:

$$\partial_t \alpha_c = (-i\omega_0 - \kappa_1) \alpha_c - i\mu \alpha_c^* + i f(x_c) \\ - \kappa_2 \alpha_c^* \alpha_c^2 - i\sqrt{2\kappa_1} \xi_1(t) - 2i\sqrt{\kappa_2} \alpha_c^* \xi_2(t). \quad (\text{F7})$$

With $\alpha_c = \sqrt{2}\alpha$ and $\xi_i = \frac{1}{\sqrt{2}}(\xi_{i,x} + i\xi_{i,p})$, we can rewrite the above Langevin equation in terms of position and momentum variables $\alpha = \frac{1}{\sqrt{2}}(x + ip)$:

$$\partial_t x = -\omega_0(\mu - 1)p - \kappa_1 x - \kappa_2(x^2 + p^2)x \\ + \sqrt{\kappa_1} \xi_{1,p} + \sqrt{2\kappa_2}(x\xi_{2,p} - p\xi_{2,x}), \\ \partial_t p = -\omega_0(\mu + 1)x + \frac{\omega_0 g^2 x}{\sqrt{2g^2 x^2/\eta + 1}} \\ - \kappa_1 p - \kappa_2(x^2 + p^2)p \\ - \sqrt{\kappa_1} \xi_{1,x} - \sqrt{2\kappa_2}(x\xi_{2,x} + p\xi_{2,p}), \quad (\text{F8})$$

where $\xi_{i,x}, \xi_{i,p}$ are independently distributed Gaussian white noises which satisfy $\langle \xi_{i,x}(t) \xi_{j,p}(t') \rangle = 0$, $\langle \xi_{i,x}(t) \xi_{j,x}(t') \rangle = \langle \xi_{i,p}(t) \xi_{j,p}(t') \rangle = \delta_{ij} \delta(t - t')$. We note that [49] studies a bosonic Hamiltonian that is equivalent to our H_- with V_{nl} expanding to the order $(a + a^\dagger)^2/\eta$. A similar set of Langevin equations is derived without the one-photon decay using the Fokker-Planck equation of the truncated Wigner function.

To obtain the analytical steady state solution for (F8), we follow a similar approach as in [49] by considering the limit where $\Delta x^2 \gg \Delta p^2$. The relative magnitude of these fluctuations can be estimated using the mean-field equation (A3). Near the critical point we assume u_p, u_x are small such that the term with coefficient γ_2 can be neglected, resulting in

$$r_f = \frac{u_x}{u_p} = \frac{(1 - \mu)^2}{\gamma_1^2}. \quad (\text{F9})$$

With $r_f \gg 1$ one can follow the same scaling analysis presented in the appendix of Ref. [49] to show that, the stochastic terms $x\xi_{2,p}, p\xi_{2,x}$ in the x -equation, $p\xi_{2,p}$ in the p -equation, and all terms containing p^2 in Eq. (F8) can

be neglected when η becomes sufficiently large. Under these approximations, Eq. (F8) reduces to:

$$\begin{aligned}\partial_t x &= -\omega_0(\mu - 1)p - \kappa_1 x - \kappa_2 x^3 + \sqrt{\kappa_1} \xi_{1,p}, \\ \partial_t p &= -\omega_0(\mu + 1)x + \frac{\omega_0 g^2 x}{\sqrt{2g^2 x^2 / \eta + 1}} \\ &\quad - \kappa_1 p - \kappa_2 x^2 p - \sqrt{\kappa_1} \xi_{1,x} - \sqrt{2\kappa_2} x \xi_{2,x}.\end{aligned}\tag{F10}$$

Since we have assumed $\omega_0^2(\mu - 1)^2 \gg \kappa_1^2$, the fluctuations in x are mainly induced by the momentum through the dominant driving term $-\omega_0(\mu - 1)p$, such that the stochastic noise $\sqrt{\kappa_1} \xi_{1,p}$ in the x -equation can be neglected. Defining $v = \partial_t x$ and substituting the p -equation into $\partial_t v$ gives:

$$\begin{aligned}\partial_t v + (2\kappa_1 + 4\kappa_2 x^2)v &= -\frac{1}{m} \partial_x U(x) \\ &\quad + \text{sgn}(T_{\text{eff}}) 2\sqrt{T_{\text{eff}}/m} (\sqrt{\kappa_1} \xi_{1,x} + \sqrt{2\kappa_2} x \xi_{2,x})\end{aligned}\tag{F11}$$

where U, T_{eff}, v are defined as in Eq. (11) of the main text.

The above stochastic equation is then equivalent to the Fokker-Planck equation of the Wigner distribution [73, 74]:

$$\begin{aligned}\partial_t W &= \left[-\partial_x v + \partial_v \left(\frac{1}{m} \partial_x U + 2(\kappa_1 + 2\kappa_2 x^2)v \right) \right] W \\ &\quad + \frac{T_{\text{eff}}}{m} 2(\kappa_1 + 2\kappa_2 x^2) \partial_v^2 W,\end{aligned}\tag{F12}$$

which yields a steady state solution in the Boltzmann form given by Eq. (10) in the main text.

Appendix G: DPTs in the inverted regime

To understand physics in the inverted regime ($\mu > \mu_c = \sqrt{1 + \gamma_1^2}$), we adopt the decoupled Master equations (8) of the main text. The corresponding MF Heisenberg equations are given by:

$$\begin{aligned}\partial_t x &= -\omega_0(\mu - 1)p - \kappa_1 x - \kappa_2(x^2 + p^2)x, \\ \partial_t p &= -\omega_0(\mu + 1)x \mp f_{\text{nl}}(x/\sqrt{\eta}) - \kappa_1 p - \kappa_2(x^2 + p^2)p,\end{aligned}\tag{G1}$$

where f_{nl} is the nonlinear force defined in the normalized MF equation for the complete model in the main text.

To gain some intuitions, we first disregard the dissipation by setting $\kappa_1 = \kappa_2 = 0$, ($\mu_c = 1$) such that:

$$\partial_t x = -\omega_0(\mu - 1)p, \quad \partial_t p = -\omega_0(\mu + 1)x \mp f_{\text{nl}}(x/\sqrt{\eta}).\tag{G2}$$

This equation can be interpreted as the equation of motion for a particle of effective mass $m_0 = -[\omega_0(\mu - 1)]^{-1}$

moving in the potential $U_0(x) = \frac{1}{2}\omega_0^2(\mu + 1)x^2 \pm V_{\text{nl}}(x)$ with V_{nl} defined in Eq. (9) of the main text. When $\mu < \mu_c$, the effective mass is positive ($m_0 > 0$), the harmonic part of $U_0(x)$ establishes a stable minimum at $x = 0$. For the (-) branch, the nonlinear potential $-V_{\text{nl}}$ counteracts against the harmonic confinement and eventually removes the minimum at the origin when g becomes sufficiently large, leading to superradiance. In contrast, when $\mu > \mu_c$, the particle exhibits a negative effective mass. The induced dynamics is physically equivalent to a particle with mass $|m_0|$ in an inverted potential $U'_0 = -U_0$, effectively reversing the roles of the harmonic and nonlinear components of the potential. In this case, V_{nl} generates the confining force and restores the minimum at $x = 0$ when g becomes sufficiently large, resulting in a transition from the SRP back to the NP. The point $\mu = \mu_c$ is identified as the critical point for spectral collapse [59], beyond which the Hamiltonian no longer supports bound states. We note that due to the stabilization effect of the two-photon dissipation, the model we investigate here always yields a stable steady state even for the case $g = 0$, $\mu > \mu_c$, where the Hamiltonian reduces to two uncoupled oscillators with PA. A second-order superradiant DPT has been identified in this decoupled model in Refs. [49, 50]. The above arguments also explain the behavior of $F_-(\bar{x})$ at different values of g in Fig. 1(b) of the main text.

Now consider the presence of one- and two-photon dissipation channels. The effective potential $U(x)$ we derived using the Langevin formalism allows us to gain a deeper understanding of the inverted regime while incorporating the effects of dissipation. With the choice of $m = 1$, we have already encoded the impact of the effective mass in the form of the potential. The critical PA strength becomes $\mu_c = \sqrt{1 + \gamma_1^2}$ as a result of the linear dissipation, which can be obtained easily by setting the coefficient of x^2 to 0. In Fig. 10 we provide four example plots of $U(x)$ that cover the ordinary ($\mu < \mu_c$) and the inverted ($\mu > \mu_c$) regime, with and without two-photon decay. When $\mu < \mu_c$, a large g turns the global minimum at $x = 0$ into a local maximum, indicating a transition from the NP to the SRP. For $\mu > \mu_c$, $\gamma_2 > 0$, it does the opposite by turning the local maximum at $x = 0$ into a global minimum, indicating a transition from the SRP to the NP. For $\mu > \mu_c$, $\gamma_2 = 0$, a large g turns the global maximum at $x = 0$ into a local minimum while the system shifts from the unstable SRP to the stable NP. The comparison between Fig. 10 (b) and (d) also visualizes how the two-photon decay stabilizes the SRP in the inverted regime by introducing a high order confining potential. We note that Fig. 10 (b),(d) are consistent with Fig. 1(b), (c) in the main text, demonstrating the equivalence between $U(x)$ and $F(\bar{x})$ in the limit $\mu - 1 \gg \gamma_1$.

For reference, we have also attached example plots of

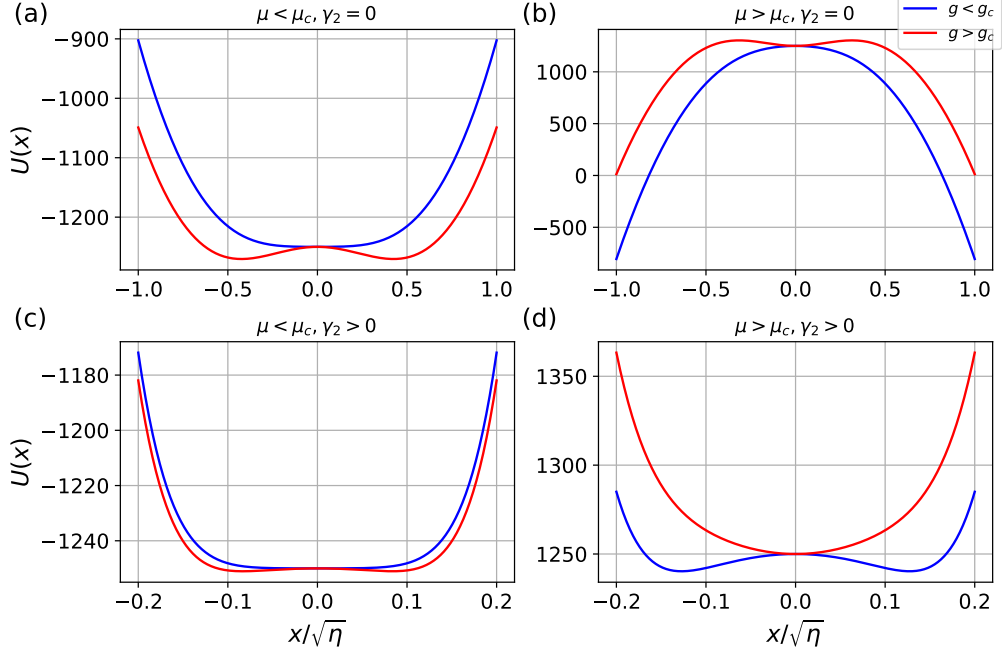


Figure 10: Effective potential $U(x)$ of the $(-)$ branch as a function of normalized coordinate $x/\sqrt{\eta}$ for different regimes. **(a,b)** are plotted without nonlinear dissipation ($\gamma_2 = 0$) while **(c,d)** assumes $\gamma_2 = 50$. **(a,c)** represent the ordinary regime $\mu = 0 < \mu_c$ while **(b,d)** represent the inverted regime $\mu = 2 > \mu_c$. The blue and red solid curves stand for the potential at $g < g_c$ and $g > g_c$. For the other parameters in the model we have used $\omega_0 = 1, \eta = 2500, \gamma_1 = 0.1$. In the ordinary regime we take $g = 1, 1.1$ while in the inverted regime we choose $g = 1.5, 2$.

$U(x)$ for the $(+)$ branch¹ in Fig. 11. In the $\mu < 1$ regime, no non-trivial local minimum exists, such that the $(+)$ branch stays in the NP. When $1 < \mu < \mu_c$, a pair of symmetric local minimum emerges when the spin-boson coupling is sufficiently large, corresponding to a super-radiant DPT at large g . Finally in the inverted regime, the potential supports no minimum with $\gamma_2 = 0$ and always supports two stable non-trivial local minimums when $\gamma_2 > 0$. This is consistent with the previous calculation that the $(+)$ branch supports no stable NP or SRP with only linear decay and stays in the SRP when the non-linear decay stabilizes the system.

As shown in Fig. 2 of the main text, the fundamentally different behaviors in the ordinary ($\mu < \mu_c$) and the inverted regimes are clearly reflected by the MF order parameters \bar{n}_{ss}, s_z . The plot for \bar{n}_{ss} can already be well explained by our analysis above. For the s_z plot, we shall notice that the spin polarization is governed by the relation $s_z = \pm \frac{1}{\sqrt{1+2g^2\bar{x}^2}}$ (from Eq. (A2)). In the ordinary regime, \bar{x} gains a non-zero value when the spin-boson coupling is strong enough to overcome the confinement generated by the amplified harmonic potential. For $g > g_c$, x grows continuously with g , resulting

in a strictly monotonic increase (decrease) in s_z for the $(-)$ ($(+)$) branch. Conversely, in the inverted regime, the spin-boson coupling acts as a confining potential for the $(-)$ branch, restricting non-zero \bar{x} solutions to the weak-coupling regime ($g < g_c$). When the transition occurs, $g\bar{x}$ jumps abruptly, pushing s_z sharply above -1 . As g decreases further, \bar{x} varies only slightly, causing $g\bar{x}$ to shrink back towards 0. This mechanism dictates the complex, non-monotonic behavior of s_z in the inverted regime, where the system ultimately mimics a return to the normal phase ($s_z \rightarrow -1$) when g vanishes.

Appendix H: Evaluation of steady-state observables

We can evaluate the steady-state expectation value of the symmetric-ordered bosonic operator $(p^k x^m)_S$ by integrating $p^k x^m W_{ss}$ over p with W_{ss} given in Eq. (10) of the main text [49]:

$$\langle p^k x^m \rangle = \left(\frac{i}{2\sqrt{2}} \right)^k \int_{-\infty}^{\infty} dx x^m H_k \left[\frac{i\sqrt{2}}{\mu-1} (\gamma_1 x + \gamma_2 x^3/\eta) \right] W_R(x), \quad (\text{H1})$$

where H_k is the Hermite polynomial and W_R is the reduced Wigner distribution:

$$W_R(x) = \int_{-\infty}^{\infty} \frac{dp}{2} W_{ss}(x, p) = \frac{1}{Z_0'} \exp(-U(x)/T_{\text{eff}}), \quad (\text{H2})$$

¹ The effective potential of the $(+)$ branch can be obtained simply by reversing the sign of V_{nl} in Eq. (11) of the main text

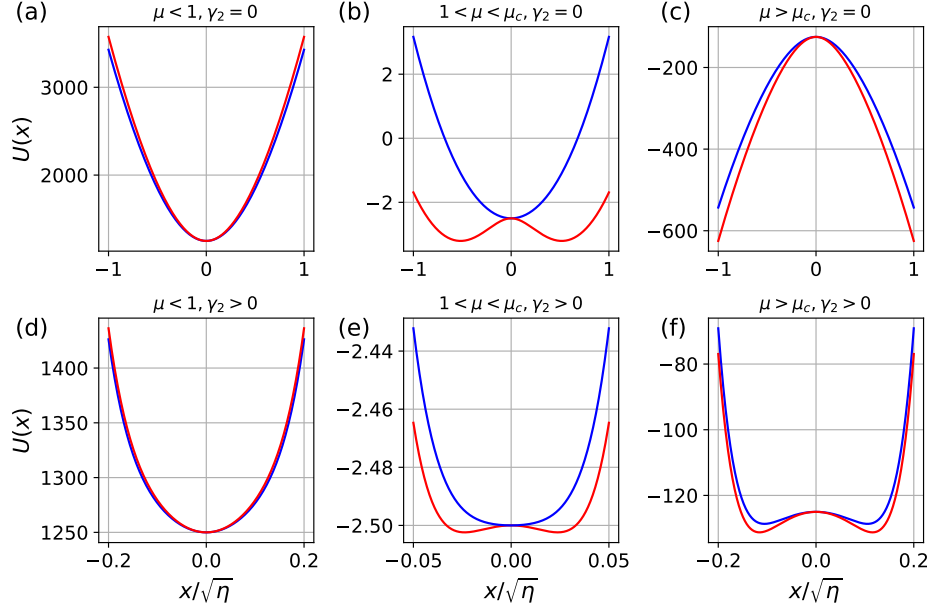


Figure 11: Effective potential $U(x)$ for the (+) branch as a function of normalized coordinate $x/\sqrt{\eta}$ for different regimes. (a,b,c) are plotted without nonlinear dissipation ($\gamma_2 = 0$) while (d,e,f) assumes $\gamma_2 = 50$. (a,c),(b,d),(c,f) represent the regimes A: $\mu = 0 < 1$, B: $1 < \mu < 1.002 < \mu_c$, C: $\mu = 2 > \mu_c$. The blue and red solid curves stand for the potential at $g < g_c$ and $g > g_c$. Here g_c is the critical coupling for the (+) branch in B and that for (-) branch in A,C. For the other parameters in the model we have used $\omega_0 = 1, \eta = 2500, \gamma_1 = 0.1$. We take $g = 1, 1.1$ in A, $g = 1, 2.5$ in B and $g = 1.5, 2$ in C.

with Z'_0 being a normalization constant. We first evaluate the critical exponent assuming $g_c \lesssim g$ but the difference $g^2 - g_c^2$ is sufficiently large compared to $1/\eta$ such that $C_2 \gg C_4$. We note that g cannot be far away from g_c , otherwise the semi-classical approximation breaks down. Evaluating the integral gives:

$$\langle x^2 \rangle = \frac{\mu - 1}{4(g^2 - g_c^2)}, \quad \langle p^2 \rangle \sim \frac{1}{4}, \quad \langle n \rangle = \frac{\mu - 1}{8(g^2 - g_c^2)} - \frac{3}{8}. \quad (\text{H3})$$

Here $\Delta x^2 = \langle x \rangle^2, \Delta p^2 = \langle p \rangle^2$ since $\langle x \rangle, \langle p \rangle = 0$ are enforced by the weak Z_2 symmetry.

We then evaluate the x, p quadratures using Eq. (H1) at the critical point $g = g_c$ such that the x^2 term in $U(x)$ vanishes. When $C_4 > 0$, the x^4 term dominates at large η such that:

$$\begin{aligned} \langle x^2 \rangle &= \frac{\Gamma(1/4)}{\Gamma(3/4)} \beta_1^{-1/2}, \\ \langle p^2 \rangle &= \frac{\gamma_1^2}{(\mu - 1)^2} \frac{\Gamma(1/4)}{\Gamma(3/4)} \beta_1^{-1/2} + \frac{1}{2} \\ \langle n \rangle &= \frac{1}{2} \left(1 + \frac{\gamma_1^2}{(\mu - 1)^2} \right) \frac{\Gamma(1/4)}{\Gamma(3/4)} \beta_1^{-1/2} - \frac{1}{4}. \end{aligned} \quad (\text{H4})$$

In the $C_4 = 0$ case (TCP), we have

$$\begin{aligned} \langle x^2 \rangle &= \frac{\sqrt{\pi}}{\Gamma(1/6)} \beta_2^{-1/3}, \quad \langle p^2 \rangle = \frac{1}{2}, \\ \langle n \rangle &= \frac{1}{2} \frac{\sqrt{\pi}}{\Gamma(1/6)} \beta_2^{-1/3} - \frac{1}{4}. \end{aligned} \quad (\text{H5})$$

Here we have defined $\beta_1 = C_4/(4T_{\text{eff}}), \beta_2 = C_6/(6T_{\text{eff}})$.

To track physics in the tricritical crossover regime while considering finite size effects, we first set $C_4 = 0$ such that the order parameter can be described by the finite-frequency scaling ansatz function $\Delta x^2 = L^\zeta F_0(\Theta)$ with $L = C_6^{-1/2}, \Theta = |g - g_c| L^{\zeta/\nu}, \zeta = 2/3, \nu = 1$ [75, 76]. To account for the effect of C_4 , we construct another dimensionless parameter Λ by taking $g = g_c$ and unifying the x^6 term in $U(x)$ with a change of variable $\tilde{x} = C_6^{1/3} x$. The dependence of $U(x)$ on C_4, C_6 is then solely encoded in a factor $\Lambda = C_4 L^{4/3}$. With these definitions we can construct the generic ansatz in Eq. (15) of the main text.

Appendix I: Higher-order multicriticality

Since $F(x)$ is in principle of infinite order, it is worth searching for multicritical points. We briefly investigate the existence of a tetracritical point. To see this, we expand $G(u_x)$ to the order of $N = 2$ to obtain a complete expression of c_6 :

$$c_6^- = \frac{1}{6(\mu - 1)^2} [2(g^2 - 2\mu)^2 \gamma_2^2 + 4g^4 \gamma_2 \gamma_1 (-1 + \mu) + 3g^6 (-1 + \mu)^3]. \quad (\text{I1})$$

The tetracritical point yields $c_2^- = c_4^- = c_6^- = 0$. Using $c_2^- = c_4^- = 0$ we can solve for γ_1, γ_2 in terms of μ, g . Substituting into to the equation $c_6^- = 0$ gives:

$$g^2 = 6\mu + 1 \pm \sqrt{24\mu^2 + 1}. \quad (\text{I2})$$

For $\mu > 1$, $g^2 > 2$, the critical condition requires $\gamma_1^2 = (\mu - 1)(-5\mu + \sqrt{24\mu + 1}) < 0$ which is impossible.

A similar conclusion can be reached by examining the effective potential $U(x)$, as the sixth order coefficient C_6 is strictly positive. It can also be observed that the two-

photon decay will not further affect higher order terms in the potential, as the highest order term that contains γ_2 is x^6 . To manipulate multicriticalities beyond tricriticality, coherent and dissipative processes of higher-order need to be introduced, such as three-photon interaction/decay.